Published October 12, 2017

Special Section: The Root Zone: Soil Physics and Beyond

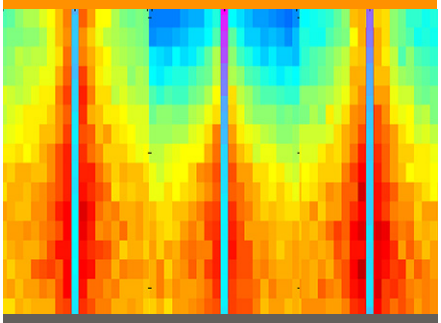

Core Ideas

- High transpiration rates lead to larger osmotic stress.
- Osmotic stress is highly dependent on root length density.
- Sinusoidal potential transpiration leads to larger stress than constant transpiration.

H. Jorda and J. Vanderborght, Dep. of Earth and Environmental Sciences, Faculty of Bioscience Engineering, Katholieke Univ. Leuven, Leuven, Belgium; A. Perelman and N. Lazarovitch, French Associates Institute for Agriculture and Biotechnology of Drylands, Jacob Blaustein Institutes for Desert Research, Ben-Gurion Univ. of the Negev, Midreshet Ben-Gurion, Israel; J. Vanderborght, Institute of Bio- and Geosciences, Agrosphere Institute, IBG-3, Forschungszentrum Jülich GmbH, Jülich, Germany. *Corresponding author (helena.jordaguerra@kuleuven.be).

Received 31 Jan. 2017.
Accepted 10 May 2017.

Citation: Jorda, H., A. Perelman, N. Lazarovitch, and J. Vanderborght. 2017. Exploring osmotic stress and differences between soil–root interface and bulk salinities. Vadose Zone J. 17:170029. doi:10.2136/vzj2017.01.0029

Exploring Osmotic Stress and Differences between Soil–Root Interface and Bulk Salinities

Helena Jorda,* Adi Perelman, Naftali Lazarovitch, and Jan Vanderborght

Design of efficient water irrigation strategies with a combination of high-quality water and saline water relies on accurate prediction of root water uptake. Macroscopic models are usually used to predict root water uptake at the field scale. However, they miss proper representation of stress processes at the plant scale. A fully mechanistic three-dimensional model was used to investigate the effect of root length density (RLD), transpiration rate and dynamics, potential leaching fraction (LF), and irrigation frequency and salinity on osmotic stress and gradients developed between the soil–root interface and the bulk soil. For the same LF and salinity level of the irrigation water, osmotic stress was larger at lower RLDs and higher transpiration rates. Roots were also more stressed when a sinusoidal transpiration boundary condition was considered. The variability of macroscopic parameters calculated for the simulated data show that macroscopic functions need to take into account RLD and transpiration rate to adequately predict osmotic stress. Finally, small salt concentration gradients were observed in this single-root study where root density was assumed constant with depth. However, future work requires checking salt concentration gradients at the scale of a whole plant, where this assumption does not apply.

Abbreviations: EC, electrical conductivity; LF, leaching fraction; RLD, root length density; SSF, standard sink fraction.

Irrigation is the main use of agricultural water and is especially important in arid and semiarid areas where precipitation is scarce and cannot fulfill the crop water requirements for the entire season. However, the availability of high-quality water, in addition to saline or sodic groundwater, is limited in such areas (Qadir et al., 2003). Thus, there has been an increasing interest in the use of saline water for irrigation. A common practice to avoid yield reduction because of saline water irrigation is to over-irrigate and avoid the accumulation of salts in the root zone. However, this leads to large amounts of drainage water with high loads of salts at concentrations higher than the initial irrigation water. The reuse of drainage water and the use of saline water is often combined with high-quality water. In such cases, different quality waters can be blended to reduce the salinity level of the irrigation water, or they can be applied at different stages of plant development or to different crops depending on their salt tolerance (Dudley et al., 2008; Groenveld et al., 2013).

Irrigation with poor-quality water presents challenges concerning the optimization of available high-quality water and the minimization of drainage water while maintaining crop growth and development. Addressing these challenges requires an accurate temporal and spatial knowledge of plant water uptake. Temporally and spatially accurate monitoring of root water uptake is time consuming and practically impossible at the scale of single roots under field conditions. Instead, modeling can be used as a tool to predict root water uptake and design appropriate irrigation schemes that can optimize the use of high-quality water while reducing leaching and maximizing crop yields.

Different modeling approaches can be used to predict plant water uptake and how it is influenced by soil water salinity. Macroscopic models commonly simulate root water

uptake in the soil as a sink term in Richards' equation. This sink term depends on a root distribution parameter and reduction functions to account for water and salinity stress. The most used stress reduction functions for water, salinity, or both stresses combined were developed in the 1970s and 1980s (Maas and Hoffman, 1977; Feddes et al., 1978; van Genuchten and Hoffman, 1984; van Genuchten, 1987; Dirksen and Augustijn, 1988). All these functions have in common the use of bulk state variables such as bulk matric potential and bulk osmotic potential. However, the accumulation of salts around the roots occurs as a result of both advective transport of salts dissolved in the water driven toward the roots by the transpiration flux and active exclusion of salts from the roots. This results in salt concentration gradients from the root–soil interface toward the bulk soil, and bulk properties, which are used in stress reduction functions, might not be representative of the water potential sensed by the root. Moreover, it has been experimentally observed that this accumulation is dependent on the transpiration rate and salinity level (Riley and Barber, 1970; Sinha and Singh, 1974, 1976). As a consequence, stress reduction functions that use bulk soil properties are situation dependent. Stress reduction functions use empirical parameters to account for the plant sensitivity to water and salinity stress, which are also known as tolerance values. However, these parameters were obtained under specific environmental conditions and mostly averaged across an entire growing season. Thus, their application to different environments and within a growing season may lead to inaccurate results. In fact, tolerance values depend on the spatial and temporal distribution of salinity along the soil profile, environmental conditions, soil factors (e.g., fertility, texture, and structure), and plant cultivar differences and breeding (Shalhevet, 1994).

In addition to macroscopic models or Type II models (Hopmans and Bristow, 2002), so-called mesoscopic models or Type I models might be used. Type I models are, in contrast to Type II models, more mechanistic and simulate flow toward single roots. For instance, de Jong van Lier et al. (2009) developed an analytical solution for combined water and salt stress based on the matric flux potential approach. Their approach estimates relative transpiration for a steady-state problem with a constant solute accumulation at the soil–root interface and does not require assumptions to derive the effect of simultaneous matric and osmotic stress. In addition, Nimah and Hanks (1973) developed a one-dimensional, numerical, mechanistic yet macroscopic model to predict root water uptake. The root extraction term per depth depends on the effective water potential in the root, the pressure and osmotic head in the soil, and the proportion of active roots at the specific depth. In addition, it is scaled by the distance from the root to where measurements of pressure and osmotic head are taken. The limitation with such models is that they assume roots to be uniformly distributed at certain depths and many have worked only for steady-state cases. Doussan et al. (1998) developed a model of root water uptake to individual roots and water transport inside the xylem of the roots that is based on the differences of potential between the soil–root interface and the root xylem and differences of potential along the root xylem segment. The models are

$$J_h(z) = -K_h \frac{d\psi(z)}{dz} \quad [1]$$

$$J_r(z) = L_r\left[\psi_s(z) - \psi_x(z)\right] \quad [2]$$

where $J_h(z)$ ($m^3\ s^{-1}$) is the flux inside the xylem at distance z from the apex, K_h is the axial conductance ($m^4\ s^{-1}\ MPa^{-1}$), $d\psi(z)/dz$ is the water potential gradient, $J_r(z)$ is the radial flux into the root from the soil per unit area ($m^3\ m^{-2}\ s^{-1}$), L_r is the radial conductivity ($m\ s^{-1}\ MPa^{-1}$), $\psi_s(z)$ is the water potential (MPa) in the soil, and $\psi_x(z)$ is the water potential inside the xylem (MPa).

The three-dimensional model R-SWMS (Javaux et al., 2008) resolves water flow in the soil using Richards' equation. Water flow in the soil is coupled through a sink term to a fully detailed three-dimensional root architectural model in which the Doussan equation (Eq. [1]) for radial root flow into the root is resolved for each individual root segment. Axial flow inside the root architecture is also resolved using the Doussan equation (Eq. [2]) and enables computing a global transpiration flux at the root collar. Models such as R-SWMS require large computational power and are unsuitable for predictions at the field scale. Nevertheless, they constitute a platform to investigate root water uptake and other processes relevant at the scale of single roots and its upscale to the whole plant (Schröder, 2014; Huber et al., 2014, 2015; Koebernick et al., 2015).

The first aim of this study was to use R-SWMS to simulate water and solute distribution at the scale of the soil volume around a single root under realistic RLDs. In the study of Schröder et al. (2013), simulations around a single root led to large total potential gradients between the soil–root interface and the bulk soil. However, their study considered only one RLD. The present study included a RLD analysis of 69 profiles, enabling the design of more realistic simulation scenarios in terms of representative soil volumes and potential transpiration associated with a single root.

Furthermore, we aimed to identify the factors affecting osmotic stress and osmotic gradients around a single root. Schröder et al. (2013) investigated the effects of salinity levels and transpiration rate on stress in a drying saline soil. Consequently, both matric and osmotic stresses were examined. In this study, to ensure the sole occurrence of osmotic stress, irrigation was applied constantly or in pulses to keep moisture high in the soil and prevent drought stress. Moreover, in addition to transpiration rate and salinity, we investigated the effects of root density, irrigation frequency, LF, and constant or transient transpiration rates on osmotic stress and the accumulation of salt around a single root.

Finally, we used these simulations to derive the link between conditions prevailing at the soil root interface and in the bulk soil.

Materials and Methods

The three-dimensional coupled mechanistic model R-SWMS (Javaux et al., 2008) was used to simulate water flow in the soil toward individual roots and along the root system. Solute transport in the soil was simulated using a particle-tracking algorithm, PARTRACE (Bechtold et al., 2011), coupled to R-SWMS as described by Schröder et al. (2013).

Root Length Density Analysis

The amount of water that is taken up by a root segment of a certain length and the average soil volume that is associated with a single root needed to be defined in our single-root simulations. To get some realistic order of magnitude of these features, we performed an analysis of RLD profiles. A database with information on 69 RLD profiles from different crops was gathered from 10 peer-reviewed studies. Table 1 gives an overview of the studies collected, the analyzed crops, and the soil type in which the crops were grown. Studies performed in artificial soils were excluded because of their influence on the development of the root system.

For the analysis, we first calculated the total root length below 1 m^2 of surface, RL_{surf} ($m\ m^{-2}$):

$$RL_{surf} = \int_{z=0}^{L_{root}} RLD(z)\,dz \qquad [3]$$

Assuming that all root segments take up the same amount of water per unit length of the root, the water uptake per unit root length, RWU_{length} ($m^3\ m^{-1}\ d^{-1}$) is

$$RWU_{length} = \frac{T}{RL_{surf}} \qquad [4]$$

where T is the transpiration rate per unit surface area ($m^3\ m^{-2}\ d^{-1}$).

To define an average distance between roots, we calculated the average root depth, $\overline{R}_{depth}$:

$$\overline{R}_{depth} = 2\frac{\int_{z=0}^{L_{root}} z\,RLD(z)\,dz}{\int_{z=0}^{L_{root}} RLD(z)\,dz} \qquad [5]$$

By dividing RL_{surf} by $\overline{R}_{depth}$, the amount of roots per square meter is obtained, from which we can derive an estimate of the average distance between root segments or average soil volume associated with one single root.

A broad range of mean root depths was obtained, and a positive correlation between mean root depth and RL_{surf} was observed (Fig. 1). A different trend was observed for the experimental samples of Kirkham et al. (1998), which were taken during dry periods. In such a case, roots grow much deeper without increasing their RLD significantly, implying that plants do not locate many roots in the shallower parts of the soil. Instead, they invest in growing fewer but longer roots to take up water from deeper soil layers. Rice (*Oryza sativa* L.) has the opposite tendency; it shows low mean root depths even at high RLD values. The effect of tillage on roots was shown in the experiments of Lampurlanés et al. (2001): crops grown in untilled soils reached higher RLD values, while the mean root depth remained similar to the other treatments. Zhang et al. (2004) showed that unirrigated winter wheat (*Triticum aestivum* L.) develops deeper roots to reach the water supply when rainfall is insufficient.

The histogram and box plot for the calculated mean root depth show that both the mean and median are ~50 cm (Fig. 2). Therefore, we took 50 cm as the average root depth for our single-root simulations. However, to reduce the simulation real time, simulations were performed with an 8-cm-long root and boundary conditions were scaled to this length. More

Table 1. Overview of the studies from which root length density (RLD) data were collected.

Study	Crop†	Soil	No. of RLD profiles
Burch et al. (1978)	soybean, sorghum	not given	5
Gao et al. (2010)	maize, soybean	loamy clay (0–15 cm), clay (15–30 cm), loamy clay (30–65 cm), sandy loam (65–100 cm)	16
Kirkham et al. (1998)	maize, soybean	silt loam (topsoil, 0–25 cm), clay horizon (25–200 cm)	8
Lampurlanés et al. (2001)	winter barley	loamy fine, mesic Fluventic Xerochrept, 0–120 cm	12
Oikeh et al. (1999)	maize	not given	3
Vamerali et al. (2009)	sugarbeet	arable layer with clay texture, tendency toward sandy loam in the deeper layers	6
Vos et al. (1998)	winter rye, forage rape	sandy soil	4
Yoshida and Hasegawa (1982)	rice	dryland	7
Zhang et al. (2004	winter wheat	deep loamy soil	2
Zotarelli et al. (2009)	tomato	sandy soil (97% sand-sized particles in upper 1 m of the profile)	6

† Barley (*Hordeum vulgare* L.); rape (*Brassica napus* L.); maize (*Zea mays* L.); rye (*Secale cereale* L.); sorghum [*Sorghum bicolor* (L.) Moench]; soybean [*Glycine max* (L.) Merr.]; sugarbeet (*Beta vulgaris* L. ssp. *vulgaris*); tomato (*Solanum lycopersicum* L.).

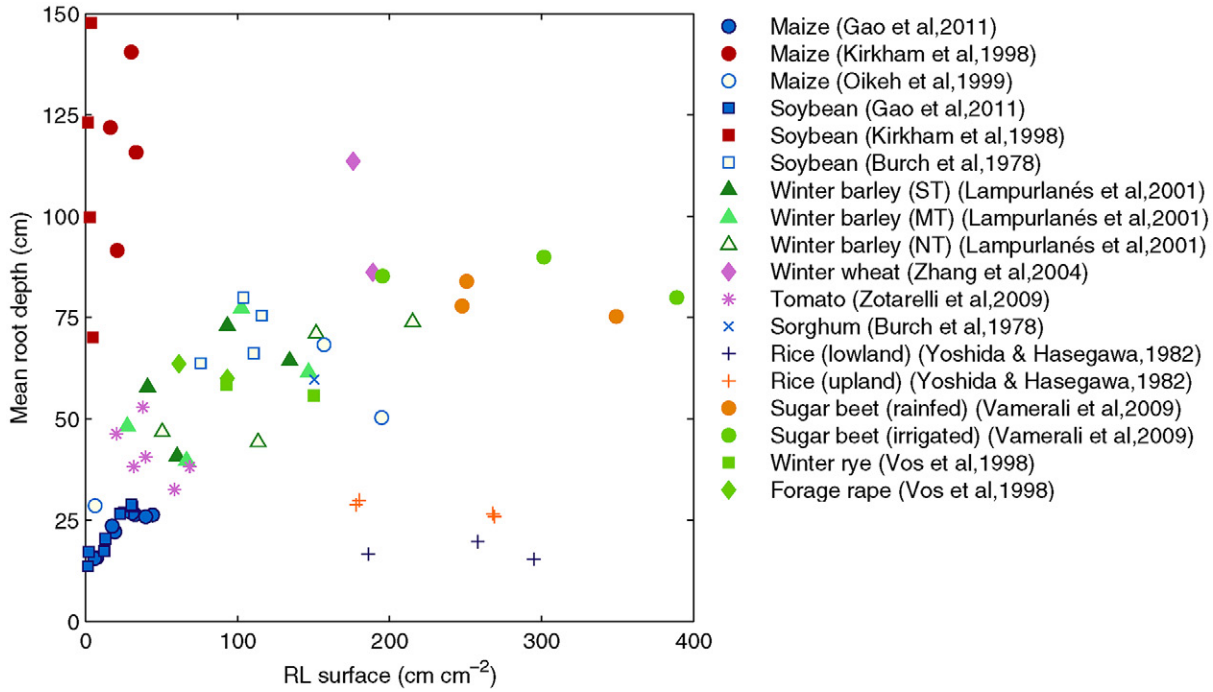

Fig. 1. Relationship between the calculated mean root depth and root length (RL) per surface unit for different crops. Winter barley received different treatments: subsoil tillage (ST), minimum tillage (MT), and no-till (NT).

information is given below. The soil surface area associated with one vertical single root varies from a few millimeters to 10s of centimeters (Fig. 3). To investigate if and how RLD plays a role in salinity gradients around a single root, we chose surface areas of 1.1, 3.6, and 14.4 cm^2 for our simulations. The smallest surface area is slightly larger than the mean area derived from these studies (0.9 cm^2).

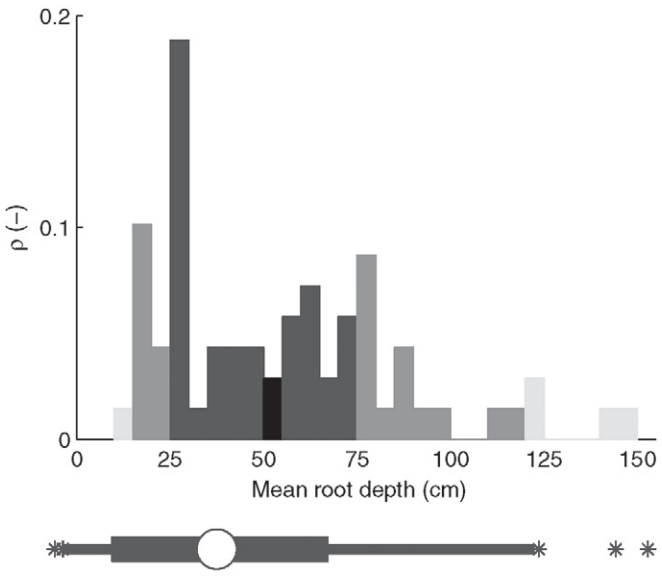

Fig. 2. Histogram and box plot for calculated mean root depth. The box plot shows the median (50.3 cm, white circle), percentiles 25 and 75 (wider bar region), percentiles 5 and 95 (narrower bar region), and outliers (stars).

Single-Root Simulations

The simulation setup consisted of an 8-cm-long root placed in the center of a soil grid with clay loam soil with hydraulic properties as summarized in Table 2. The root hydraulic parameters and the model setup are presented in Table 3. Irrigation water with different salinity levels was applied homogenously on the top of the profile, and a free drainage boundary condition was set at the bottom (Table 4).

We designed a series of simulation scenarios to study the effect of different factors on osmotic stress and on the osmotic gradients developed around a single root. These factors are (i) RLD, (ii) potential transpiration (magnitude and dynamics), (iii) irrigation frequency, (iv) salinity in the irrigation water, and (e) LF. The LF is defined as the ratio of the amount of water draining out of the root zone to the water amount infiltrated into the soil's surface.

Root Length Density

We performed simulations with different grid dimensions to study the effect of three RLD values. For an average RLD, a 1.05- by 1.05- by 10-cm grid (1.1 cm^2 surface area per root) with a discretization of 0.05 cm in the horizontal dimension and 0.5 cm along the z axis was defined. For a low RLD, we defined a 1.9- by 1.9- by 10-cm grid (3.6 cm^2 surface area per root) with 0.1- and 0.5-cm discretization in the horizontal and vertical dimensions, respectively. Finally, for a very low RLD, a 3.8- by 3.8- by 10-cm grid (14.4 cm^2 surface area per root) with a 0.2-cm discretization in the horizontal direction and 0.5 cm along the z axis was defined. A previous simulation study with different spatial resolution was

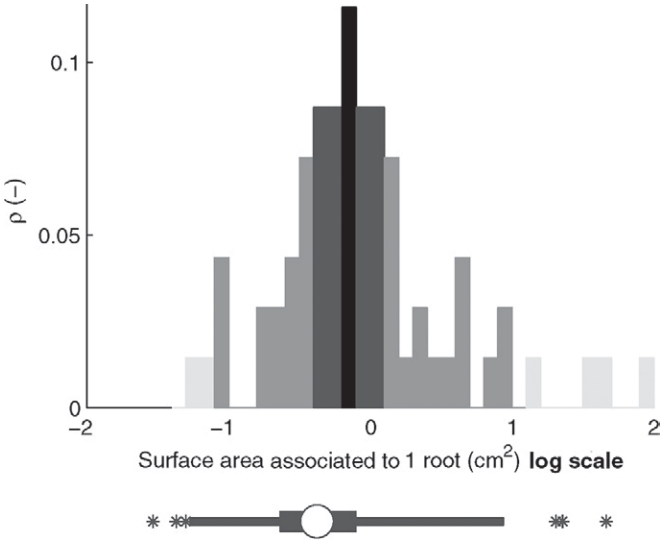

Fig. 3. Histogram and box plot for calculated surface area (in logarithmic scale, base 10) associated with one single root. The box plot shows the median (−0.1224; white circle), percentiles 25 and 75 (wider bar region), percentiles 5 and 95 (narrower bar region), and outliers (stars).

conducted, and, at the scale of this work, the different horizontal discretizations were not relevant for the results.

The reason for running simulations under very low RLD is that osmotic stress mostly occurs in arid and semiarid geographical areas. Under these climatic conditions, plants invest in growing fewer but deeper roots to find sources of water, thus leading to low RLD profiles (Ho et al., 2005; Lynch, 2007). In addition, salt levels are generally the highest at the fringes of the root zone, for instance, at the bottom of the root zone. In such areas, root densities are also lower.

Potential Transpiration

Both the dynamics and the intensity of potential transpiration were studied. Transpiration was applied both as a constant as well as a daily sinusoidal boundary condition at the root collar. Furthermore, three different potential transpiration rates were applied, namely 0.32, 0.8, and 1.28 mm d^{-1} (scaled for the 8-cm-long root, which corresponds to 2, 5, and 8 mm d^{-1} for a whole plant; see Table 5).

Both transpiration rate and the limit total water potential at the root collar, which causes the plant to switch from constant transpiration rate to constant water potential, were adjusted to the 8-cm-long root. Because an average root depth of 50 cm was found, a realistic transpiration rate can be calculated multiplying by a factor 8/50 (the ratio between an 8-cm-long root segment over an average 50-cm-long root). For the limit collar potential, we also multiplied the commonly used value of −15,000 cm by the factor 8/50. This was based on the assumption that the main loss in water potential as a result of flow in the root system occurs in the axial direction. Although the resistance to flow in the axial direction is generally much smaller than in the radial direction, the length of the flow path is much larger in the axial direction. This may lead to considerable water potential losses along the axial direction. However, it must be noted that this assumption is an extreme one, so that a more realistic value would lie in between. The choice of this limit collar potential will define the effects in a quantitative way, but it will not affect in a qualitative way the relationships between the studied factors and stress.

Table 2. Soil water retention characteristics† of the clay loam (Carsel and Parrish, 1988).

θ_r	θ_s	a	n	K_s	l	ρ_b
		cm^{-1}		cm d^{-1}		g cm^{-3}
0.095	0.41	0.019	1.31	6.24	0.5	1.44

† θ_r, residual volumetric water content; θ_s, saturated volumetric water content; α and n, fitting parameters; K_s, saturated hydraulic conductivity; l, connectivity–tortuosity coefficient; ρ_b, bulk density.

Table 3. Root morphologic and water conductivity characteristics. Root hydraulic characteristics (K_r and K_x) were obtained from Doussan et al. (1998)

Root characteristic		Value	Units
Length		8	cm
No. of segments		20	–
Length each segment		0.4	cm
Root length density (RLD)	Very low RLD	0.069	cm cm^{-3}
		1.1	cm^2 per root
	Low RLD	0.277	cm cm^{-3}
		3.6	cm^2 per root
	Avg. RLD	0.907	cm cm^{-3}
		14.4	cm^2 per root
Radial conductivity (K_r)		0.0001728	cm s^{-1} cm^{-1}
Xylem conductivity (K_x)		0.0432	cm^4 s^{-1} cm^{-1}

Irrigation Frequency

Three different irrigation frequency schemes were applied: irrigation was kept constant for a constant boundary condition, whereas

Table 4. Boundary conditions in the soil.

	Boundary condition			
Boundary	Water			Solute
Top	constant irrigation	irrigation every 3 d (3-d pulse)	irrigation every 7 d (1-wk pulse)	constant conc. in irrigation water
Bottom	free drainage	free drainage	free drainage	zero gradient
Right, left, face, back	no flow	no flow	no flow	zero gradient

Table 5. Potential transpiration and irrigation rates for the scenarios with different root length densities (RLDs) and leaching fractions (LFs).

Potential transpiration	Transpiration rate			Irrigation			
	Very low RLD	Low RLD	Avg. RLD	LF = 0.05	LF = 0.25	LF = 0.7	LF = 0.85
mm d^{-1}	$cm^3 d^{-1}$			mm d^{-1}			
0.32	0.035	0.166	0.462	0.337	0.427	1.067	2.133
0.8	0.088	0.289	1.155	0.842	1.067	2.667	5.333
1.28	0.141	0.462	1.848	1.347	1.707	4.267	8.533

for transient simulations, irrigation was applied in pulses of 1-d duration once every 3 or 7 d, respectively. The total amount of water irrigated for the entire simulation period was the same for the three irrigation scenarios. The rates are given in Table 5.

Salinity in Irrigation Water

We applied five salinity treatments in the irrigation water: 5, 10, 15, 20, and 25 μmol cm^{-3}. These correspond to electrical conductivities (ECs) of approximately 0.5, 1, 1.5, 2, and 2.5 dS m^{-1}, respectively. Irrigation water with up to 0.7 dS m^{-1} EC does not need restriction in use, whereas ECs between 0.7 and 3 dS m^{-1} require from slight to moderate restriction (Ayers and Westcot, 1985). Sodium was considered the solute, and the root membrane was assumed to be impermeable to Na^+ (reflection coefficient σ = 1). This is a reasonable assumption based on a comparison between experimental data and simulations by Schröder et al. (2013). Osmotic potential inside the xylem was neglected, which implies that any plant osmotic adjustment was also neglected. Osmotic potentials were obtained from solute concentrations according to

$$h = \beta c \quad [6]$$

where β was −50 μmol^{-1} cm^4, as in Schröder et al. (2013).

Potential Leaching Fraction

For all scenarios, different LFs were applied and the corresponding irrigation rates were implemented. The LFs that we defined refer to the ratio of the leaching out of the soil volume around the considered root segment to the amount of water that flows into this soil volume. This is different from LFs that are normally defined for the entire root zone. If we regard our 8-cm-long root segment as part of a 50-cm-long root, different LFs should be applied depending at which depth this segment is placed, since more water leaches from soil volumes around root segments that are closer to the surface to supply water to the roots that are deeper. Hence, we decided to investigate different LF values depending on the position of this segment: at the top of the root system (LF = 0.85), mid-depth (LF = 0.7), and at the end of the root system (LF = 0.25).

Note that the designed LFs were used to calculate irrigation rates assuming that the actual transpiration equals potential transpiration. If there is osmotic stress, water uptake will be reduced and thus LFs calculated from the system will be higher than the designed ones. For this reason, we will refer to the designed LFs as potential LFs.

As initial conditions for all scenarios, we applied a pressure head of −100 cm in the whole soil domain and a homogeneous salt concentration equal to the concentration in the irrigation water. The simulation time was 100 d, and output was obtained once a day. To evaluate daily dynamics, output was obtained 10 times per day at uniform intervals for a limited amount of simulation time.

Calculation of Soil–Root Interface and Bulk Potentials

Soil–root interface and bulk osmotic, matric, gravitational, and total potentials were averaged along the length of the root segment using the standard sink fraction (SSF) defined by Couvreur et al. (2012) as a weighting factor. Couvreur et al. (2012) developed a new three-dimensional macroscopic model for root water uptake based on analytical solutions of water flow in a simple root system. This model takes into account the hydraulic architecture of the root, that is, the network of radial and axial conductance of all segments of the root system:

$$T_{act} = K_{rs}\left(\sum_{j=1}^{M} H_{si,j}\mathrm{SSF}_j - H_{collar}\right) \quad [7]$$

where T_{act} is the actual transpiration; K_{rs} is the global conductance of the root system; $H_{si,j}$ is the total potential at the soil–root interface for the jth segment, that is, the sum of the elevation, pressure, and osmotic heads; H_{collar} is the root collar potential; and SSF_j is the standard sink fraction of the jth segment, which corresponds to the fraction of water taken up by the jth segment under uniform water potential. The sum of $H_{si,j}\mathrm{SSF}_j$ for all root segments is, therefore, the soil–root interface potential sensed by the root.

Results and Discussion

An instance of the simulation results is shown in Fig. 4, where the solute concentration distribution in an x–z plane containing the root and radial root flow are plotted. After an irrigation event, salts are flushed out and transpiration recovers, especially on the top segments of the root system. For a low potential LF (Fig. 4a–4c), after

an irrigation event, salt at the edges of the profile are flushed out, while more salt remains at the soil–root interface driven by the transpiration flux. On the other hand, under high potential LF (Fig. 4d–4f), the irrigation flux is large enough to homogenize the profile completely and to reduce salt accumulation around the root. Figure 4 thus shows the relevance of accounting for transient conditions as well as the irrigation rate to estimate the amount of salt that can accumulate around a single root.

Relationship between Osmotic Stress and Analyzed Factors

The ratio of actual to potential cumulative transpiration, the α_{stress} or stress factor (Feddes et al., 1978; van Genuchten, 1987; Homaee et al., 2002), was used to compare the degree of stress experienced by the root under different combination of factors. The α_{stress} ranges from 0 to 1, 0 being the highest stress felt by the plant (no transpiration occurs) and 1 being a no-stress situation. In the studied scenarios, stress was mainly caused by low osmotic potentials; matric potentials remained fairly high throughout the entire simulation time because of frequent irrigation. Therefore, we can interpret α_{stress} as exclusively a result of osmotic stress.

Osmotic stress was negatively correlated to RLD (Fig. 5). Under very low RLD (Fig. 5a), the root experienced stress even under low salinity levels and low transpiration rate. Lower RLD implies larger evaporative demand per unit root length, which leads to larger stress. These results support our motive for running simulations under very low RLD. Our simulations also confirm that stress is larger when the root is exposed to a high evaporative demand, high salinity, and low potential LF. High evaporative demands lead to faster accumulation of salt around the root, reaching the potential limit for the onset of

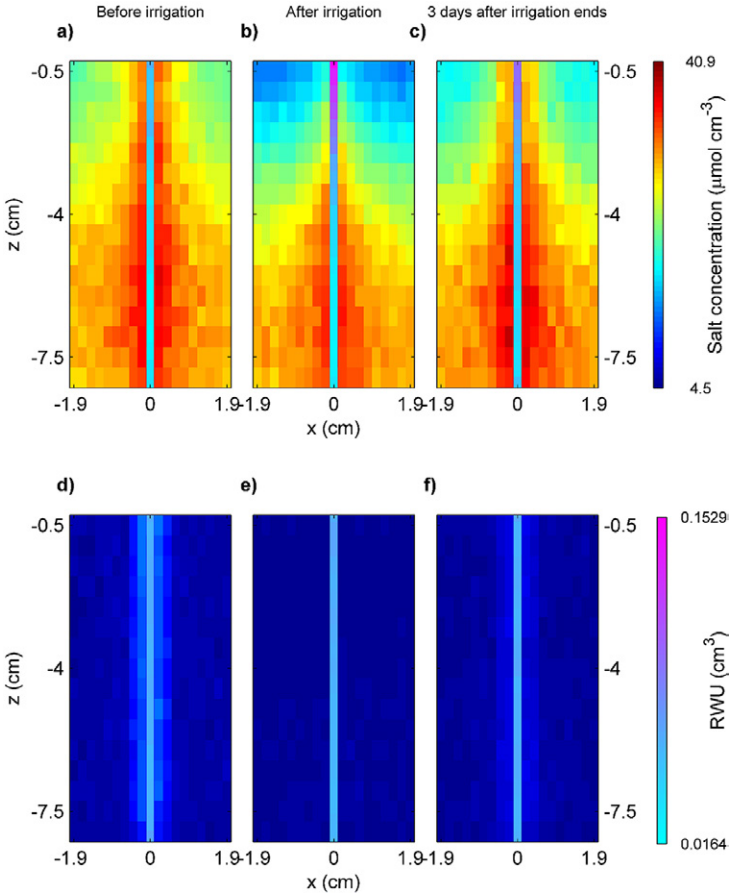

Fig. 4. Solute distribution concentration and radial root flow for three different time steps for the x–z plane that contains the root system under the scenario of very low root length density, medium constant transpiration rate, 1-wk pulse irrigation, and 5 µmol cm^{-3}, with a potential leaching fraction of (a,b,c) 0.05 or (d,e,f) 0.85. The color bar located at the top right refers to the solute concentration in the soil, while the color bar at the bottom right corresponds to root water uptake (RWU) per segment. The root can be identified in each plot as the vertical line located in the center.

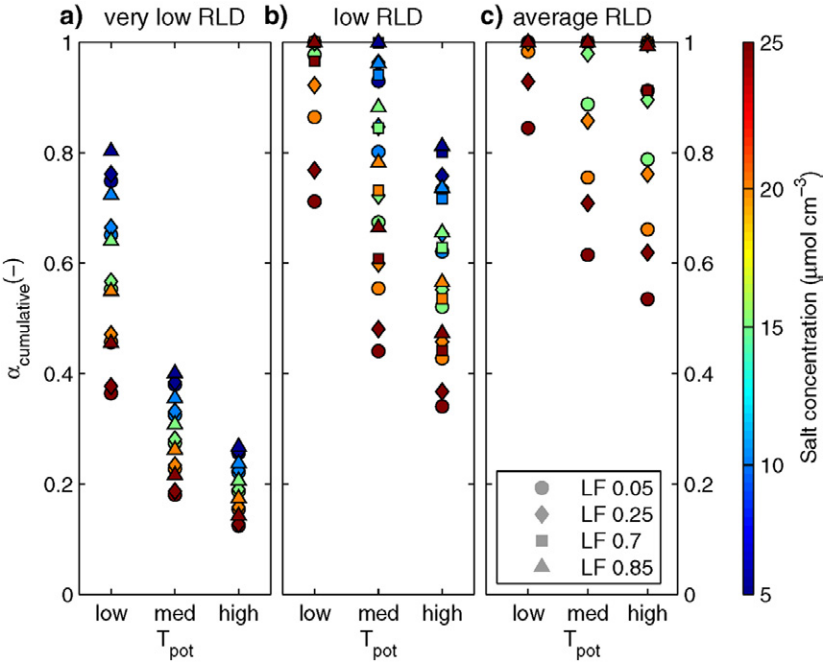

Fig. 5. Cumulative stress factor, α_{stress}, at the end of the simulation period for a constant irrigation scheme, sinusoidal potential transpiration (T_{pot}), different leaching fractions (LFs), and (a) very low root length density (RLD), (b) low RLD, and (c) average RLD.

stress earlier; whereas high potential LFs flush the salts out of the profile and slow down the process of salt accumulation around the root, thus delaying the onset of stress. High potential LFs are more likely to occur at the top of the root system where the RLD is usually larger. The coupled effect of high potential LF and large RLD leads to low levels of transpiration stress. On the contrary, at the bottom of a root system, LFs are usually lower because of water uptake in upper zones of the root system. Therefore, combined low RLDs with low LFs end up in large levels of stress.

Irrigation frequency (constant or as a 3-d or 1-wk period) did not affect the degree of stress significantly (data not shown). Finally, we observed that stress was larger when a sinusoidal potential transpiration was imposed at the root collar (Fig. 6a). Sinusoidal transpiration reaches larger rates during midday than constant transpiration, thus leading to larger stress. In addition, these differences in stress were larger for very low and low RLD scenarios. For very low RLD scenarios, differences were the largest at low potential transpiration (Fig. 6b). At higher values of potential transpiration, the plant was highly stressed under both constant or sinusoidal evaporative demand, leading to smaller stress differences. However, in low RLD scenarios, the largest differences occurred at both high potential transpiration under low salinity and medium potential transpiration under high salinity (Fig. 6c). For larger evaporative demands and salinities, the plant was highly stressed under both constant and sinusoidal evaporative demand, causing the difference in stress to decrease. Conversely, under low evaporative demand, the plant was moderately stressed for both constant and sinusoidal potential transpiration, also leading to small differences in stress.

These results show that stress reduction functions must take into account not only daily averaged transpiration rates but also its daily dynamics. Dynamics are important not only at large evaporative demand and salinities but also, and sometimes most importantly, at low evaporative demand and low salinities.

Differences between Soil–Root Interface and Bulk Potentials

The results of our simulations showed small osmotic potential differences between the soil–root interface and the bulk soil. In scenarios with constant irrigation, the differences were small as a result of the constant washing out of salts from the profile. In pulse irrigation scenarios, differences were also modest and experienced a dynamic behavior. This behavior was controlled by the potential LF of the scenario. For low potential LFs, such as 0.05, the osmotic potential difference between the soil–root interface and the bulk soil increased right after the pulse irrigation (Fig. 7a). Under such conditions, osmotic stress is larger, leading to a decrease in transpiration. Although we can observe an accumulation of salt around the root, there was also a large amount of salts in the bulk soil (Fig. 4a). As irrigation occurs, salts are flushed down the profile, stress is reduced, and root water uptake increases, which drives water and

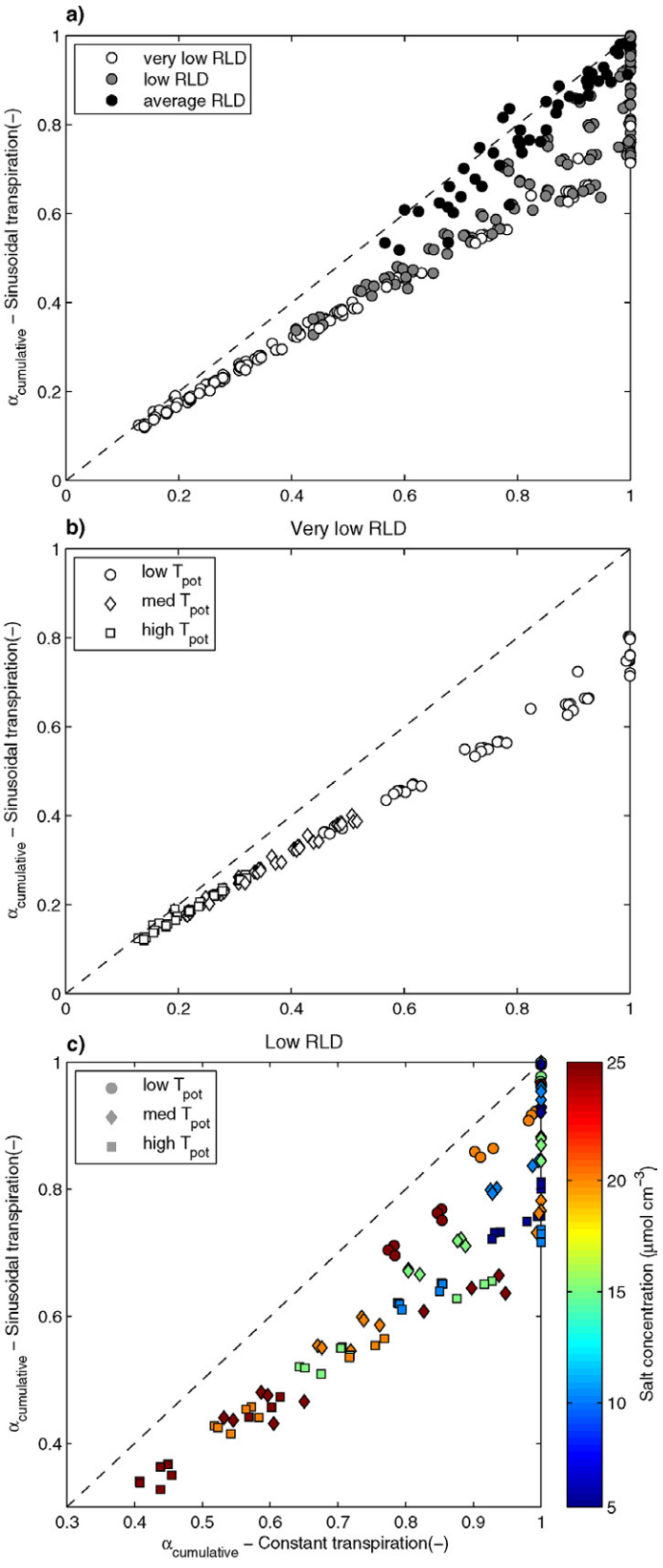

Fig. 6. Comparison of cumulative stress factor, α_{stress}, for simulations under constant transpiration and sinusoidal transpiration: (a) all data colored according to their root length density (RLD); (b) only data from the very low RLD scenario and symbols according to the potential transpiration rate (T_{pot}); and (c) data from the low RLD scenario colored according to salinity and symbols according to the T_{pot}.

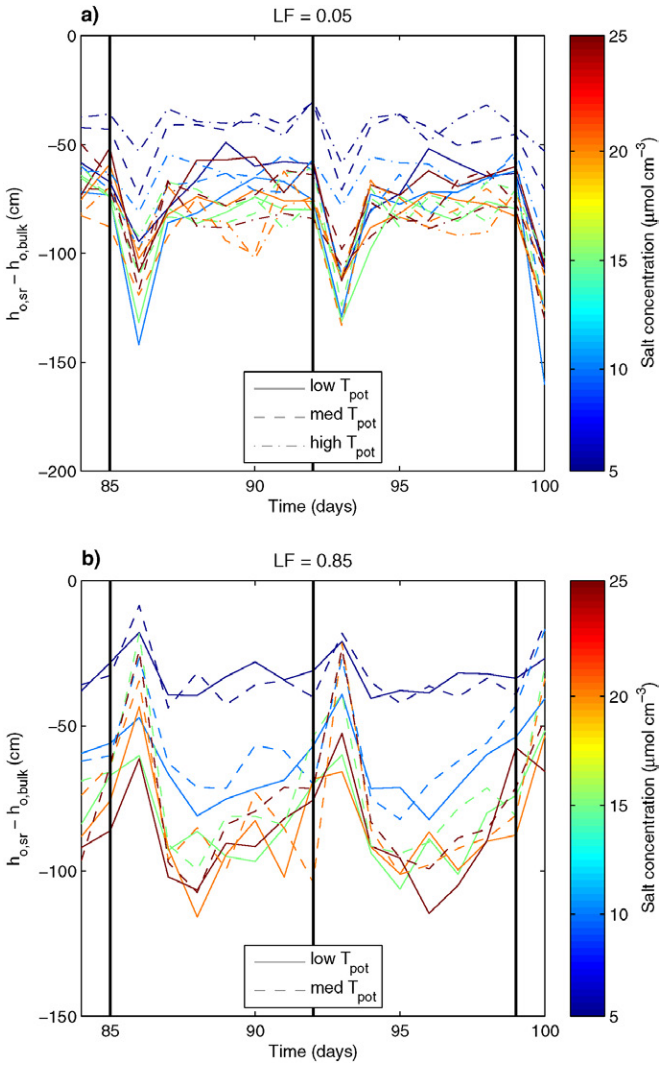

Fig. 7. Time series (80–100 d) of osmotic difference between the soil–root interface ($h_{o,sr}$) and the bulk soil ($h_{o,bulk}$) for very low root length density (RLD) scenarios (3.8- by 3.8-cm grid) and 7-d pulse irrigation for different potential transpiration rates (T_{pot}) and potential leaching fractions (LFs) of (a) 0.05 and (b) 0.85. Irrigation pulses are indicated by thick black vertical lines.

therefore solute toward the root surface. As a consequence, the salt flushing is less effective near the root surface than in the bulk soil (see also Fig. 4b). Consequently, although the absolute osmotic stress around the root is lower, there is a greater difference between the soil–root interface and the bulk soil. In contrast, when the potential LF is high (0.85), the irrigation pulse homogenizes the profile and reduces the concentration gradient between the soil–root interface and the bulk soil (Fig. 4d–4f and 7b).

In addition to dynamic behavior because of pulse irrigation, daily variability because of sinusoidal transpiration was also observed. Figure 8 depicts the 2-d time series of total, matric plus gravitational, and osmotic potentials at the soil–root interface and bulk soil for a

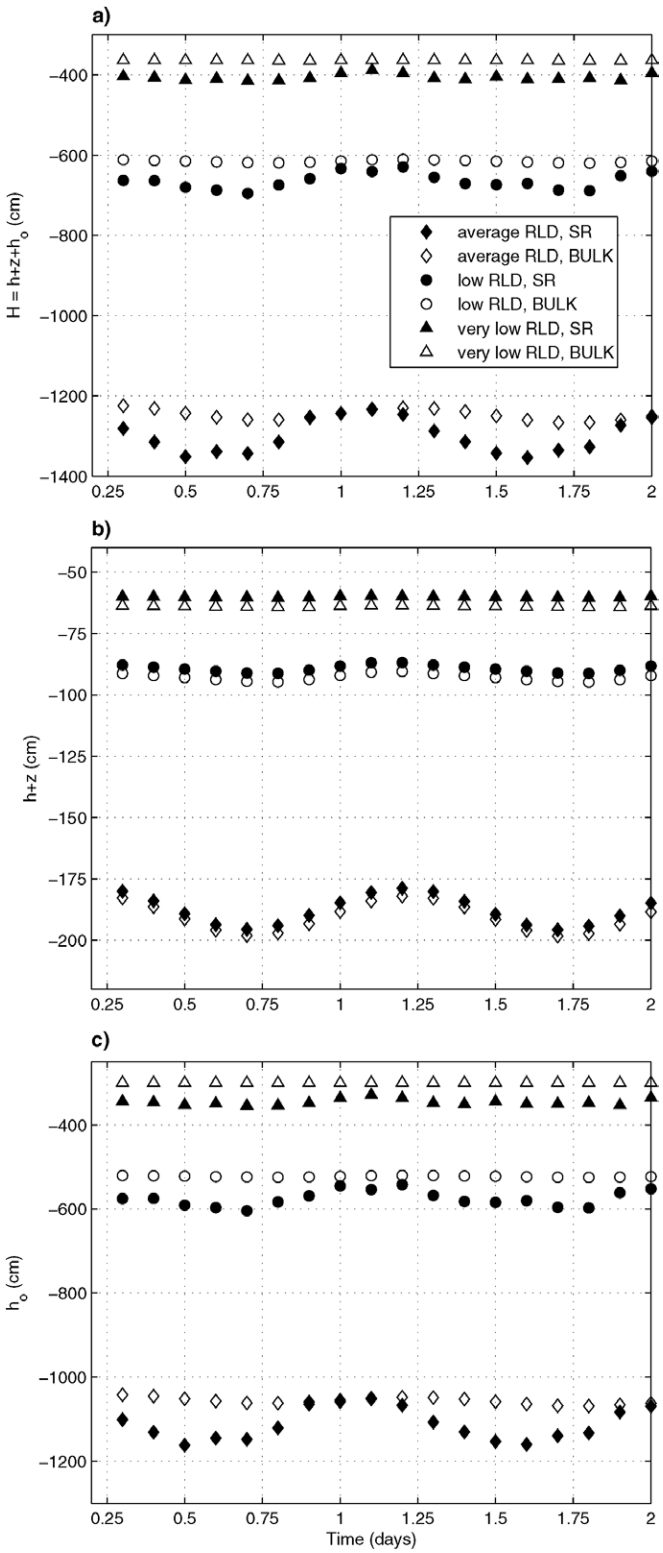

Fig. 8. Time series of (a) total, (b) matric plus gravitational, and (c) osmotic potential at the soil–root interface (SR) and in the bulk soil (BULK) for the constant-irrigation scenario with a potential leaching fraction (LF) of 0.25. Data shown for average, low, and very low root length density (RLD) under low evaporative demand and a salinity level of 5 µmol cm^{-3}.

constant-irrigation scenario. Several observations can be made from this figure. First, the total potential was mostly made up of osmotic potential; consequently, we can establish that the stress experienced by the plant was essentially osmotic. Second, both bulk and soil–root interface potentials were found to be more negative in average RLD simulations while becoming less negative with decreasing RLD. This is related to the level of stress and consequent effect on actual LFs. In very low RLD scenarios, very large potential transpiration fluxes are imposed at the root collar. To reach such transpiration fluxes, the potential at the root collar needs to decrease to the level for stress onset and transpiration decreases. In consequence, actual LFs are much larger than potential LFs, and large amounts of salt are leached out of the root zone. This leads to lower amounts of salts accumulated in the soil and the root zone, although stress remains high. On the contrary, in average RLD scenarios, stress is lower or zero, LFs are equal to or slightly higher than the potential ones, and more salt accumulates in the root zone, leading to lower water potentials. Because the potential transpiration fluxes at the collar are lower, even at such low total water potentials, the potential transpiration rate can completely or almost completely be reached. This explains why salinity is higher in the average RLD scenarios, which are exposed to less stress, while being lower in more stressed scenarios in very low RLD simulations. This is pictured in Fig. 9a, where actual transpiration is plotted as a function of SSF-averaged soil–root interface total potential. Under high evaporative demand, such as in very low RLD scenarios, potential transpiration cannot be reached because the maximum gradient between SSF-average soil–root total potential and root collar potential is not large enough to result in the desired transpiration rate. In such cases, the transpiration rate could only be reached by increasing the root hydraulic properties (K_{rs}) (see Eq. [7] and Fig. 9b). For instance, a 10-fold increase in both radial conductivity and axial conductance allows higher potential transpiration rates to be achieved in very low RLD scenarios, thus decreasing the stress felt by the plant (Fig. 9b). Contrary to the very low RLD scenarios, actual transpiration for an average RLD can be met even at higher absolute values of total soil–root interface potential.

Third, the soil–root interface osmotic potential was always lower than the bulk soil osmotic potential in very low RLD scenarios, exhibiting an accumulation of salt around the root compared with the bulk soil at all times (Fig. 8c). Conversely, for low and average RLDs, osmotic potential was lower at the soil–root interface than in the bulk soil only during high evaporative demand (midday = 0.5, 1.5 d), whereas the soil–root interface and bulk potentials were quasi-equal during low evaporative demand (night = 0, 1, 2 d). Soil matric plus gravitational potential exhibited the same daily dynamics both at the soil–root interface and in the bulk soil and increasing or decreasing with the same order of magnitude (Fig. 8b). A negative gradient of matric plus gravitational potential toward the soil–root interface was maintained throughout the simulation time, indicating a positive flow of water from the soil toward the root as a result of the transpiration flow. Osmotic potential at the soil–root interface presents

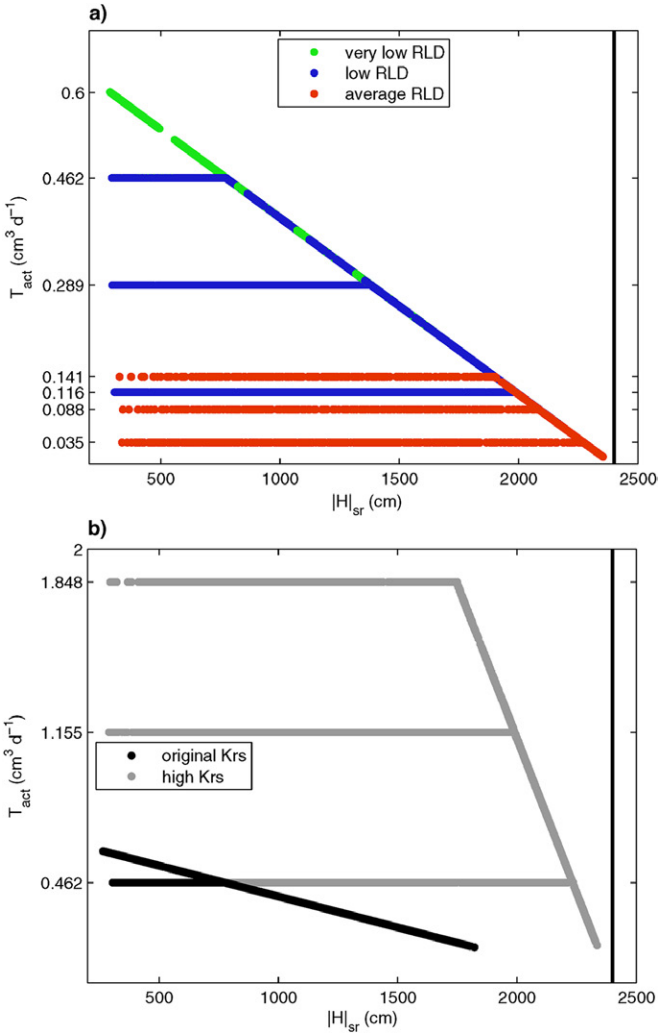

Fig. 9. Actual transpiration rate (T_{act}) as a function of total potential at the soil–root interface averaged with standard uptake fraction (SUF) and absolute total water potential ($|H|$). Low, medium, and high transpiration rates at average root length density (RLD) are 0.035, 0.088, and 0.141 cm^3 d^{-1}, respectively; those at low RLD are 0.116, 0.289, and 0.462 cm^3 d^{-1}, respectively; and those at very low RLD are 0.462, 1.155, and 1.848 cm^3 d^{-1}, respectively. The vertical line indicates a potential of −2400 cm, at which transpiration would stop. Simulation results for (a) global root conductivity $K_r = 1.728 \times 10^{-4}$ cm s^{-1} cm^{-1} and xylem conductivity $K_x = 4.32 \times 10^{-2}$ cm^4 s^{-1} cm^{-1}, and (b) very low RLD scenarios compared with the original combination of root conductivities (black) and radial and axial conductivities 10 times larger (gray).

a larger oscillation than in the bulk soil (Fig. 8c), indicating that dynamic potential transpiration causes greater local variations of salt concentration at the soil–root interface than in the bulk soil. This supports the importance of differentiating between properties at the rhizosphere and in the bulk soil: bulk soil potential measurements would not be able to account for the daily variability of the potential sensed by the plant.

Variability of Macroscopic Parameters

Data on bulk osmotic potential and α_{stress} were used to fit the macroscopic model of van Genuchten and Hoffman (1984):

$$\alpha_{stress}(h_o) = \frac{1}{1+(h_o/h_{o50})^p} \quad [8]$$

where h_o is the bulk osmotic potential, h_{o50} is the osmotic potential at which transpiration is reduced by half, and p is a shape parameter. The parameter h_{o50} is a measure of the sensitivity or tolerance of the plant to salinity stress. A plant with very negative values of h_{o50} is highly tolerant to salinity, while one with less negative h_{o50} values is highly sensitive. The shape parameter p describes the steepness of the curve. Larger p values lead to steeper curves, which means that stress increases fast across small intervals of bulk osmotic potential. An example of fitted data is shown in Fig. 10 (black data).

Our results show that both h_{o50} and p are highly dependent on RLD and potential transpiration rate. Therefore, we plotted h_{o50} and p as a function of potential transpiration flux, expressed as the volume of water imposed at the root collar per time, which combines both the transpiration rate (usually expressed as the volume of water transpired per soil surface and time) and RLD (Fig. 11). The macroscopic parameter h_{o50} was found to be less negative (more sensitive to salinity) with increasing potential transpiration flux (i.e., increasing transpiration rate and decreasing RLD; Fig. 11a), which agrees with what was discussed above. In addition, the shape parameter p was negatively correlated with the potential transpiration flux (Fig. 11b). This would imply a more gradual increase in stress in high-stressed scenarios (very low RLD and high transpiration rate), while an abrupt decrease in transpiration is more common in less-stressed scenarios.

Macroscopic parameters are usually computed as single values for each crop and used for the entire growing season. However, our study shows that both h_{o50} and p are highly dependent on both potential transpiration and RLD. Thus, the inclusion of such factors in macroscopic functions is necessary to accurately predict the effect of salinity on root water uptake.

Finally, we examined how macroscopic parameters vary depending on whether osmotic bulk potential or osmotic soil–root interface potential is used to fit the data ($h_{o50,bulk}$ and $h_{o50,sr}$, respectively). Absolute values of h_{o50} were slightly larger when osmotic soil–root interface potential data were used to fit the macroscopic function (Fig. 10). This means that plant tolerance to salinity expressed as h_{o50} is apparently larger when osmotic soil–root interface potentials are used to calculate this parameter. In Fig. 12, a plot of the difference between $h_{o50,bulk}$ and $h_{o50,sr}$ divided by $h_{o50,bulk}$ as a function

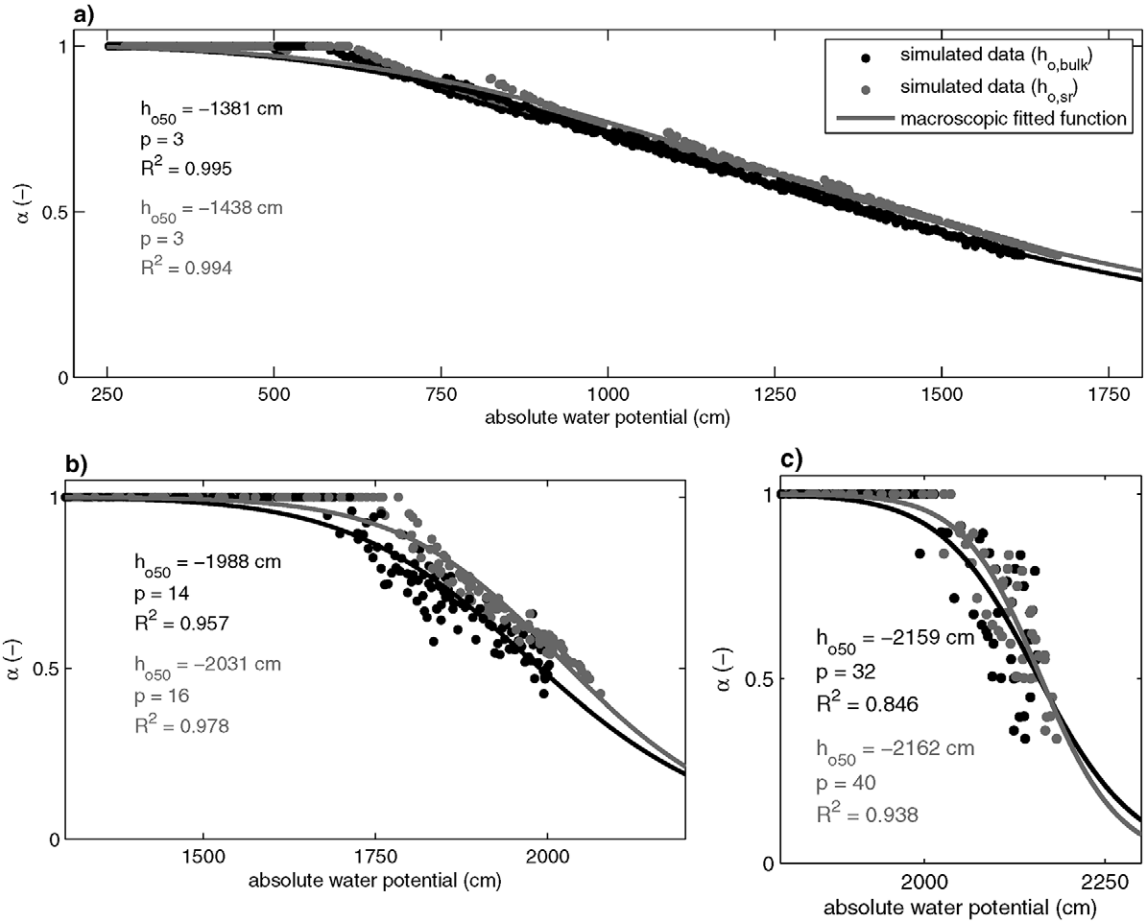

Fig. 10. Macroscopic fitting of simulated data for (a) very low root length density (RLD), (b) low RLD, and (c) average RLD under constant irrigation, constant low transpiration rate, and a potential leaching fraction of 0.05. Both osmotic bulk potential ($h_{o,sr}$) and osmotic soil–root interface potential ($h_{o,bulk}$) were used to fit the macroscopic function.

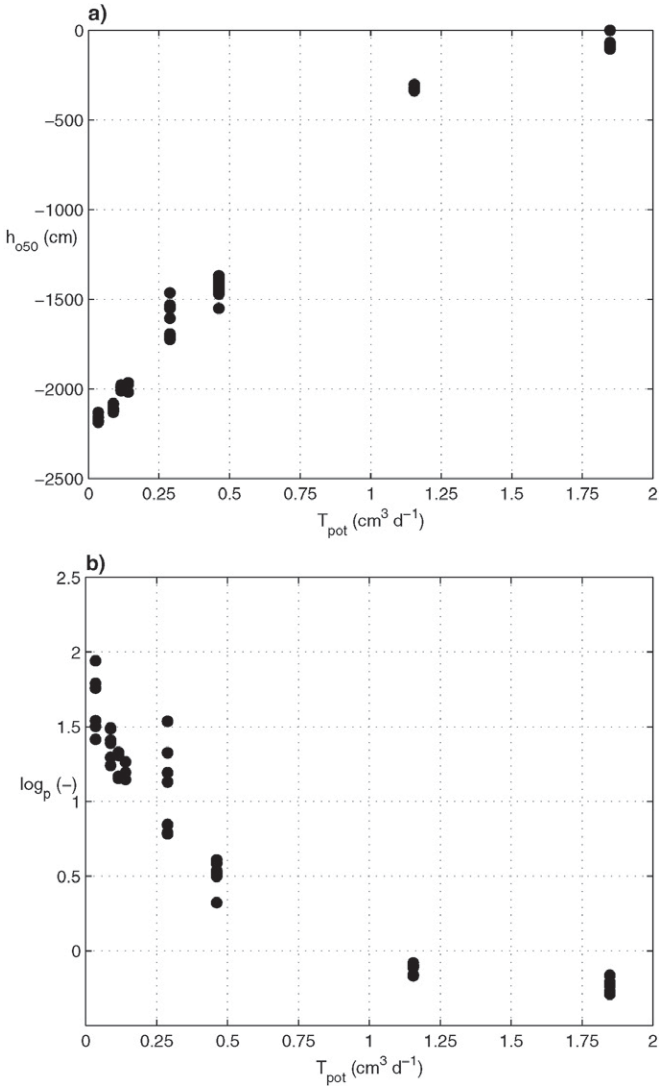

Fig. 11. Macroscopic parameters calculated from (a) the bulk osmotic potential h_{o50} and (b) p dependence on potential transpiration flux (T_{pot}, volume of water imposed at the root collar per unit time).

of potential transpiration flux ($cm^3\ d^{-1}$) is presented. The relative difference was found to be moderately positively correlated to the potential transpiration flux. The larger the transpiration flux, the larger the relative difference between the macroscopic parameters, which indicates that the relative difference between the bulk osmotic potential and the osmotic potential at the soil–root interface is positively correlated to the transpiration rate and negatively correlated to RLD. This is consistent with previous studies, where a larger accumulation of salt around the root was found at larger transpiration rates (Sinha and Singh, 1974, 1976; Schröder et al., 2013). However, the scattered data at large transpiration rates indicate that irrigation scheduling and rate also play a role.

Conclusions

Synthetic experiments were conducted for a range of atmospheric conditions, RLDs, and irrigation water quality and frequency using

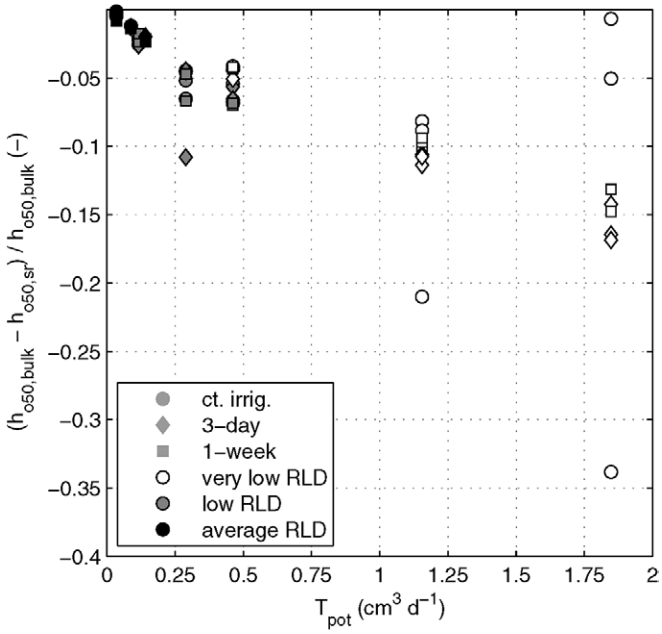

Fig. 12. Relative difference among osmotic potentials h_{o50} calculated from bulk osmotic potential and bulk soil–root interface potential data for a range of potential transpiration (T_{pot}) under constant (ct.), 3-d interval, and 1-wk interval irrigation and very low, low, and average root length density (RLD).

a three-dimensional, physically based model that resolves flow and transport to individual root segments and couples water flow in the soil and root system. The effect of salt concentrations on root water uptake was accounted for by including osmotic water potential gradients between the solution at the soil–root interface and the root xylem sap in the hydraulic gradient between the soil and root.

Results from the simulations indicate that osmotic stress is highly dependent on RLD. Low RLDs result in a greater stress to the plant because of a high evaporative demand per root unit length. In addition, osmotic stress is positively correlated to the potential transpiration rate. Sinusoidal potential transpiration leads to larger stress than constant transpiration because high transpiration rates are imposed at the root collar during midday. Potential LF was found to be negatively correlated to osmotic stress. Low LFs lead to higher stress because less salt is leached out of the profile, resulting in higher salinity levels in the soil. The dependency of osmotic stress on the studied factors was also observed when computing the macroscopic parameters for the stress function developed by van Genuchten and Hoffman (1984). Plant salt tolerance, expressed as the bulk osmotic potential that leads to a reduction in half of the transpiration, h_{o50}, was larger (smaller in absolute value) under high evaporative demand and lower RLD. In addition, the shape parameter p was found to be highly dependent on RLD and evaporative demand. According to our results, the shape of the stress curve, which is defined by p, is steeper under larger RLD and low transpiration rate. Time-variant macroscopic parameters based on knowledge of the current potential transpiration rate per root unit length would be more convenient to accurately predict osmotic stress during a growing season.

The single-root analysis is based on the assumption of homogeneous RLD at a certain depth in the soil profile. Under this assumption, small osmotic gradients between the soil–root interface and the bulk soil are expected. Salt accumulation at the soil–root interface, compared with the bulk soil, was slightly larger for very low RLDs and also during midday when a sinusoidal transpiration is imposed. However, future work requires checking salt concentration gradients at the scale of a whole plant, where root density varies with depth and is not homogeneous at one specific depth.

Acknowledgments

This work has been funded by IWT-Vlaanderen (Project IWT 141353). This research was also supported by a grant from the German–Israeli Foundation for Scientific Research and Development, I-1231-204.12/2014.

References

Ayers, R.S., and D.W. Westcot. 1985. Water quality for agriculture. FAO, Rome.

Bechtold, M., J. Vanderborght, O. Ippisch, and H. Vereecken. 2011. Efficient random walk particle tracking algorithm for advective–dispersive transport in media with discontinuous dispersion coefficients and water contents. Water Resour. Res. 47:W10526. doi:10.1029/2010WR010267

Burch, G.J., R.C.G. Smith, and W.K. Mason. 1978. Agronomic and physiological responses of soybean and sorghum crops to water deficits: II. Crop evaporation, soil water depletion and root distribution. Funct. Plant Biol. 5:169–177.

Carsel, R.F., and R.S. Parrish. 1988. Developing joint probability distributions of soil water retention characteristics. Water Resour. Res. 24:755–769. doi:10.1029/WR024i005p00755

Couvreur, V., J. Vanderborght, and M. Javaux. 2012. A simple three-dimensional macroscopic root water uptake model based on the hydraulic architecture approach. Hydrol. Earth Syst. Sci. 16:2957–2971. doi:10.5194/hess-16-2957-2012

de Jong van Lier, Q., J.C. van Dam, and K. Metselaar. 2009. Root water extraction under combined water and osmotic stress. Soil Sci. Soc. Am. J. 73:862–875. doi:10.2136/sssaj2008.0157

Dirksen, C., and D. Augustijn. 1988. Root water uptake function for non-uniform pressure and osmotic potentials. In: 1988 Agronomy abstracts. ASA, Madison, WI. p. 188.

Doussan, C., L. Pagès, and G. Vercambre. 1998. Modelling of the hydraulic architecture of root systems: An integrated approach to water absorption: Model description. Ann. Bot. 81:213–223. doi:10.1006/anbo.1997.0540

Dudley, L.M., A. Ben-Gal, and N. Lazarovitch. 2008. Drainage water reuse: Biological, physical, and technological considerations for system management. J. Environ. Qual. 37:S-25–S-35. doi:10.2134/jeq2007.0314

Feddes, R.A., P.J. Kowalik, and H. Zaradny. 1978. Simulation of field water use and crop yield. PUDOC, Wageningen, the Netherlands.

Gao, Y., A. Duan, X. Qiu, Z. Liu, J. Sun, J. Zhang, and H. Wang. 2010. Distribution of roots and root length density in a maize/soybean strip intercropping system. Agric. Water Manage. 98:199–212. doi:10.1016/j.agwat.2010.08.021

Groenveld, T., A. Ben-Gal, U. Yermiyahu, and N. Lazarovitch. 2013. Weather determined relative sensitivity of plants to salinity: Quantification and simulation. Vadose Zone J. 12(4). doi:10.2136/vzj2012.0180

Homaee, M., C. Dirksen, and R.A. Feddes. 2002. Simulation of root water uptake: I. Non-uniform transient salinity using different macroscopic reduction functions. Agric. Water Manage. 57:89–109. doi:10.1016/S0378-3774(02)00072-0

Ho, M.D., J.C. Rosas, K.M. Brown, and J.P. Lynch. 2005. Root architectural tradeoffs for water and phosphorus acquisition. Funct. Plant Biol. 32:737–748. doi:10.1071/FP05043

Hopmans, J.W., and K.L. Bristow. 2002. Current capabilities and future needs of root water and nutrient uptake modeling. Adv. Agron. 77:103–183. doi:10.1016/S0065-2113(02)77014-4

Huber, K., J. Vanderborght, M. Javaux, N. Schröder, I. Dodd, and H. Vereecken. 2014. Modelling the impact of heterogeneous rootzone water distribution on the regulation of transpiration by hormone transport and/or hydraulic pressures. Plant Soil 384:93–112. doi:10.1007/s11104-014-2188-4

Huber, K., J. Vanderborght, M. Javaux, and H. Vereecken. 2015. Simulating transpiration and leaf water relations in response to heterogeneous soil moisture and different stomatal control mechanisms. Plant Soil 394:109–126. doi:10.1007/s11104-015-2502-9

Javaux, M., T. Schröder, J. Vanderborght, and H. Vereecken. 2008. Use of a three-dimensional detailed modeling approach for predicting root water uptake. Vadose Zone J. 7:1079–1088. doi:10.2136/vzj2007.0115

Kirkham, M.B., S.J. Grecu, and E.T. Kanemasu. 1998. Comparison of minirhizotrons and the soil–water-depletion method to determine maize and soybean root length and depth. Eur. J. Agron. 8:117–125. doi:10.1016/S1161-0301(97)00019-1

Koebernick, N., K. Huber, E. Kerkhofs, J. Vanderborght, M. Javaux, H. Vereecken, and D. Vetterlein. 2015. Unraveling the hydrodynamics of split root water uptake experiments using CT scanned root architectures and three dimensional flow simulations. Front. Plant Sci. 6. doi:10.3389/fpls.2015.00370

Lampurlanés, J., P. Angás, and C. Cantero-Martınez. 2001. Root growth, soil water content and yield of barley under different tillage systems on two soils in semiarid conditions. Field Crops Res. 69:27–40. doi:10.1016/S0378-4290(00)00130-1

Lynch, J.P. 2007. Roots of the second Green Revolution. Aust. J. Bot. 55:493–512. doi:10.1071/BT06118

Maas, E.V., and G. Hoffman. 1977. Crop salt tolerance: Current assessment. J. Irrig. Drain. Div., Am. Soc. Civ. Eng. 103:115–134.

Nimah, M.N., and R.J. Hanks. 1973. Model for estimating soil water, plant, and atmospheric interrelations: I. Description and sensitivity. Soil Sci. Soc. Am. J. 37:522–527. doi:10.2136/sssaj1973.03615995003700040018x

Oikeh, S.O., J.G. Kling, W.J. Horst, V.O. Chude, and R.J. Carsky. 1999. Growth and distribution of maize roots under nitrogen fertilization in plinthite soil. Field Crops Res. 62:1–13. doi:10.1016/S0378-4290(98)00169-5

Qadir, M., T. Boers, S. Schubert, A. Ghafoor, and G. Murtaza. 2003. Agricultural water management in water-starved countries: Challenges and opportunities. Agric. Water Manage. 62:165–185. doi:10.1016/S0378-3774(03)00146-X

Riley, D., and S.A. Barber. 1970. Salt accumulation at the soybean (*Glycine max.* (L.) Merr.) root–soil interface. Soil Sci. Soc. Am. Proc. 34:154–155. doi:10.2136/sssaj1970.03615995003400010042x

Schröder, N. 2014. Three-dimensional solute transport modeling in coupled soil and plant root systems. Forschungszentrum Jülich, Jülich, Germany.

Schröder, N., N. Lazarovitch, J. Vanderborght, H. Vereecken, and M. Javaux. 2013. Linking transpiration reduction to rhizosphere salinity using a 3D coupled soil–plant model. Plant Soil. 377:277–293. doi:10.1007/s11104-013-1990-8

Shalhevet, J. 1994. Using water of marginal quality for crop production: Major issues. Agric. Water Manage. 25:233–269. doi:10.1016/0378-3774(94)90063-9

Sinha, B.K., and N.T. Singh. 1974. Effect of transpiration rate on salt accumulation around corn roots in a saline soil. Agron. J. 66:557–560. doi:10.2134/agronj1974.00021962006600040023x

Sinha, B.K., and N.T. Singh. 1976. Salt distribution around roots of wheat under different transpiration rates. Plant Soil 44:141–147. doi:10.1007/BF00016962

Vamerali, T., M. Guarise, A. Ganis, and G. Mosca. 2009. Effects of water and nitrogen management on fibrous root distribution and turnover in sugar beet. Eur. J. Agron. 31:69–76. doi:10.1016/j.eja.2009.03.005

van Genuchten, M.Th. 1987. A numerical model for water and solute movement in and below the root zone. US Salinity Lab., Riverside, CA.

van Genuchten, M.Th., and G. Hoffman. 1984. Analysis of crop production. In: I. Shainberg and J. Shalhevet, editors, Soil salinity under irrigation: Processes and management. Ecol. Stud. 51. Springer, New York. p. 258–271.

Vos, J., P.E.L. van der Putten, M.H. Hussein, A.M. van Dam, and P.A. Leffelaar. 1998. Field observations on nitrogen catch crops. Plant Soil 201:149–155. doi:10.1023/A:1004367530320

Yoshida, S., and S. Hasegawa. 1982. The rice root system: Its development and function In: Drought resistance in crops with emphasis on rice. IRRI, Los Baños, Laguna, Philippines. p. 97–114.

Zhang, X., D. Pei, and S. Chen. 2004. Root growth and soil water utilization of winter wheat in the North China Plain. Hydrol. Processes 18:2275–2287. doi:10.1002/hyp.5533

Zotarelli, L., J.M. Scholberg, M.D. Dukes, R. Muñoz-Carpena, and J. Icerman. 2009. Tomato yield, biomass accumulation, root distribution and irrigation water use efficiency on a sandy soil, as affected by nitrogen rate and irrigation scheduling. Agric. Water Manage. 96:23–34. doi:10.1016/j.agwat.2008.06.007